Bacteria Size Determination by Elastic Light Scattering

A. Katz, Alexandra Alimova, Min Xu, Elizabeth Rudolph, Mahendra K. Shah, Howard E. Savage, Richard B. Rosen, Steven A. McCormick, and Robert R. Alfano, *Fellow, IEEE*

***Abstract*—Light extinction and angular scattering measurements were performed on three species of bacteria with different sizes and shapes (*Pseudomonas aeruginosa, Staphylococcus aureus,* and *Bacillus subtilis*). The Gaussian Ray approximation of anomalous diffraction theory was used to determine the average bacteria size from transmission measurements. A rescaled spectra combining multiple angular data was analyzed in the framework the Rayleigh–Gans theory of light scattering. Particle shape and size distribution is then obtained from the rescale spectra. Particle characteristics (size and/or shape) retrieved from both methods are in good agreement with size and shape measured under scanning electron microscopy. These results demonstrate that light scattering may be able to detect and identify microbial contamination in the environment.**

***Index Terms*—Microorganism detection, optical extinction, optical scattering.**

I. Introduction

CURRENT methods for identifying and classifying bacteria involve isolating a specimen and growing the bacteria in culture media for 24–48 h in order to obtain an adequate population. Typically, bacteria are stained and identified under microscopic examination. A real-time *in situ* identification method would be a significant advance in monitoring the environment for microbial contamination and would allow rapid response to biological contamination and prevent spread of disease. With the recent threat of bioterrorism, optical approaches have the potential to detect the spread of different types of microorganisms and are being investigated. Light scattering may be able to provide a real-time technology to detect and classify different bacteria genera based on size and shape. Light scattering measurements do not need large populations for detection. In point of fact, data analysis is more straightforward for concentrations sufficiently dilute so as to avoid multiple scattering events. Over thirty years ago, Wyatt [1] discussed the feasability of using of light scattering to identify bacterial cells, "The characteristic of each distinct microorganism that scatters is an essentially unique scattering pattern" due to the distinct biochemical nature and structure of each microorganism.

The light-scattering properties of bacteria, human cells and tissues have been investigated for both purposes of species identification and for determination of cell status. It has been shown that the Rayleigh–Gans (R–G) theory agrees with measurements of angular distribution of scattered light intensity from bacteria [2], [3]. The refractive index and cell dimensions have been correlated with light scattering measurements [4], [5] and light scattering has been employed to look at the structure of a single bacteria [6]. Mie scattering theory has been applied to model bacteria growth patterns. [7] Polarized light scattering at 633 nm was used to measure average size distributions of bacteria [8]. Changes of bacteria size in growth media was investigated using polarized light scattering [9]. Forward scattering from cell suspensions was used to relate the scattering properties to internal cell structures [10]. More recently, there have been investigations into using light scattering from human tissues and cells in order to detect changes indicative of malignancy [11]–[13].

Cells can be classified as either eukaryotic (Fungi, Plantae, and Animalia kingdoms) or prokaryotic (Monera kingdoms, i.e., bacteria and blue-green algae). Eukaryotic cells are larger in size (10–100 microns) and contain a membrane-bound nucleus with chromosomes, DNA and proteins, mitochondria, and organelles. Prokaryotic cells are typically smaller in size (0.2–10 μm for bacteria) than eukaryotes and are characterized by the lack of nuclear organization and the complex organelles present in eukaryotic cells. [14] The scattering centers of mammalian cells consist of many different structures and organelles found within the cells [15] with potential scatterings being: nuclei, on the order of 3–10 μm; mitochondria, 1–4 μm long and 0.3–0.7 μm wide; and lysosomes, spherical in shape with 0.2–0.5 μm diameter [16]. The scattering properties of prokaryotic cells will depend more on the size, shape, and index of refraction of the cell than on internal cell structures. In point of fact, standard laboratory practice employs optical density to estimate microbe concentration. Most of the common bacteria generally come in a few different shapes: spheres, rods, short rods, and spirals. Their sizes are such that the angular and wavelength distribution of scattered light is strongly dependent on the size and shape of the microbes.

Manuscript received November 15, 2002; revised February 5, 2003. This work was sponsored in part by grants from the New York State Office of Science, Technology and Academic Research (NYSTAR), a NASA University Research Center Grant, the National Oceanic and Atmospheric Administration, the New York Eye and Ear Pathology Research Fund, the New York Eye and Ear Infirmary Ophthalmology Chairman's Research Fund, the Achelis-Bodman Foundation, and the Lowenstein Foundation. The work of M. Xu was sponsored by the U. S. Army under Grant #DAMD17-02-1-0516.

A. Katz, A. Alimova, M. Xu, and R. R. Alfano are with the Institute for Ultrafast Spectroscopy and Lasers, The City College of New York, New York, NY 10031 USA (e-mail: akatz@ccny.cuny.edu).

E. Rudolph is with the Department of Earth and Atmospheric Science, The City College of New York, New York, NY 10031 USA.

M. K. Shah, H. E. Savage, and S. A. McCormick are with the Department of Pathology, New York Eye and Ear Infirmary, New York, NY 10003 USA.

R. Rosen is with the Department of Ophthalmology, New York Eye and Ear Infirmary, New York, NY 10003 USA.

Digital Object Identifier 10.1109/JSTQE.2003.811284

TABLE I
LIST OF ACRONYMS AND ABBREVIATIONS

R-G	Rayleigh-Gans (approximation of scattering)
GRA	Gaussian Ray Approximation
ADT	Anomalous Diffraction Theory
IC	Intermediate Case (of scattering)
PSD	Particle Size Distribution
m	Relative Refractive Index
x	Size Parameter (equal to $2\pi a/\lambda$)
Pa	*Pseudomonas aeruginosa*
Sa	*Staphylococcus aureus*
Bs	*Bacillus subtilis*

In this paper, the transmission and angular distribution of scattered light were measured from three species of bacteria with differences in size and shape. The transmission measurements were analyzed to determine the average particle size and to determine the absorption and scattering contributions to the extinction coefficient. The angular distribution of scattered light was analyzed to determine the particle size distribution of the bacteria and the aspect ratio for the rod-shaped bacteria.

Acronyms and symbols used in this paper are listed in Table I.

II. THEORY

The usual approach to the scattering problem is to make appropriate approximations to light scattering by small particles depending on size parameter and relative refraction index [17], [18]. The size parameter x is defined as $2\pi r/\lambda$, where r is the "dimension" of the object and the relative refraction index is the ratio of the index of the scatterer to the index of the surrounding media. For spherical objects, r is the radius. For soft particles, such as bacteria, the R–G approximation is applicable when the phase shift inside the particle is small ($2x|m-1| \ll 1$). Soft particles are those particles whose relative refractive index is close to unity ($|m-1| \ll 1$). Anomalous diffraction theory (ADT) becomes valid for $x \gg 1$. The R–G and the ADT overlap in the region where the conditions $x \gg 1$ and $x|m-1| \ll 1$ are satisfied, the "so-called" intermediate case (IC) of light scattering.

A. Gaussian Ray Approximation

The ADT is a powerful tool for approximating scattering from spherical and nonspherical particles [17]. The Gaussian ray approximation (GRA) was recently shown to be useful as a statistical interpretation of ADT [19]. In the GRA, the scattering cross section in the absence of absorption can be approximated by

$$C_{\rm sc} = G\left[\frac{4n^2\pi^2}{\lambda^2}(m-1)^2\left(\mu^2+\sigma^2\right) - \frac{4n^4\pi^4}{3\lambda^4}(m-1)^4\left(\mu^4+3\sigma^4+6\mu^2\sigma^2\right)\right] \quad (1)$$

where G is the geometric cross section, $\mu = \langle l\rangle$ is the mean light path through the scatterer and σ is given by

$$\sigma^2 = \langle l^2\rangle - \langle l\rangle^2. \quad (2)$$

This approximation is valid for soft particles with a medium size parameter ($5 \le x \le 50$). A range which includes most microorganisms for scattering with visible light. The valid range of the size parameter extends substantially if the particles are polydisperse. In the long wavelength limit, the second term in (1) is negligible and the GRA reduces to the IC.

Using the GRA on randomly oriented particles, the mean geometric path and mean square root geometrical ray path, averaged over all particle orientations and weighted by their respective geometrical cross sections, can be determined by light extinction measurements. This provides a measure of the sizes of all particles involved. The nominal particle size can then be deduced from the mean geometric path and mean square root geometrical ray path, provided the particle shape is known. In this case, knowledge of concentration is not necessary. In the IC limit of the GRA, however, concentration information is required to obtain particle size, due to the absence of the second term in (1).

In the IC and the large size limit of R–G, the total scattering cross sections for spheres and cylinders are given by [17], [18]

$$\begin{aligned} C_{sc}(\text{sphere}) &= \frac{8n^2\pi^3}{\lambda^2}|m-1|^2 r^4 \\ C_{sc}(\text{cylinder}) &= \frac{32n^2\pi^3}{3\lambda^2}|m-1|^2 r^3 l \\ &\quad (\text{random orientation},\ l >> r) \end{aligned} \quad (3)$$

where r is the radius of the sphere or cylinder, l is the length of the cylinder, n is the index of the surrounding media, and λ is the wavelength in vacuum. It is assumed that the cylinders are randomly oriented.

B. Transmission

For medium in which both scattering and absorption is present, the ballistic light intensity I_B is given by

$$I_B(\lambda) = I_0(\lambda)e^{-C_{\rm sc}(\lambda)NL - C_{\rm abs}(\lambda)NL} \quad (4)$$

where $C_{\rm sc}$ is the scattering cross section, $C_{\rm abs}$ is the absorption cross section, N is the concentration, and L is the optical path length. In the absence of absorption, the total scattered fluence is the difference between the incident fluence and the transmitted fluence.

In transmission measurements, the light incident on the detector consists of both the true ballistic light and the fraction of scattered light incident within the detector collection angle, θ_D. When a highly collimated illumination source is used, θ_D can be made small by increasing the sample to detector distance. However, with white light illumination, beam divergence will limit the sample to detector distance. For samples with low scattering and absorption, I_B is relatively large while the total scattered light intensity ($I_{\rm TS}$) is small and the detected signal is composed

almost entirely of ballistic light. The optical density (OD) is then given by

$$OD = -\log_{10}\left(\frac{I_T}{I_0}\right) = \ln(10) \times (C_{\rm sc} + C_{\rm abs})\, NL. \quad (5)$$

For highly scattering samples, I_B is small while $I_{\rm TS}$ is large and the detected signal will consist of both ballistic light and light which is scattered within the detector collection angle. In this situation, the measured OD will deviate from being proportional to concentration and be smaller than its true value. The OD at which forward scattering light leakage becomes noticeable depends on particle size, as scattering from larger particles is concentrated more at smaller angles.

Due to the range of wavelengths available in this paper, only the leading term of $C_{\rm sc}$ in the GRA was observed in the transmission measurements for the smaller sized bacteria. For these particles, the scattering contribution to the OD is approximately proportional to λ^{-2} and approaches zero in the long wavelength limit. From the expression given for the scattering cross section (3) the OD for spherical particles is given by

$$OD = \log(10)\left(\frac{8n^2\pi^3}{\lambda^2}|m-1|^2 r^4 NL + C_{\rm abs} NL\right) \quad (6)$$

and for cylindrical particles by

$$OD = \ln(10)\left(\frac{32n^2\pi^3}{3\lambda^2}|m-1|^2 r^3 lNL + C_{\rm abs} NL\right). \quad (7)$$

The particle size be can calculated from the following expressions for spheres

$$r^4 = \frac{2.303M}{8n^2 NL\pi^3|m-1|^2} \quad (8)$$

and cylinders

$$r^3 l = \frac{2.303 \times 3M}{32n^2 NL\pi^3|m-1|^2} \quad (9)$$

where a is the bacteria cell radius, l is the bacteria cell length, N is the concentration, and M is the slope of OD plotted as a function of $1/\lambda^2$. The evaluation of (8) or (9) requires *a priori* knowledge of the concentration and shape in order to calculate particle size.

For larger bacteria investigated in this study, the second term in (1) provides an appreciable contribution to the extinction and the OD can be fitted by a function of the form

$$OD = \frac{A_0}{\lambda^2} + \frac{A_1}{\lambda^4}. \quad (10)$$

From (1) and (2), the bacteria size can then be obtained without the knowledge of the concentration.

Single scattering is not assumed for particle sizing from transmission measurements. This may provide some advantage in real-time environmental monitoring.

C. Angular Scattering

For single scattering in the R–G approximation, the angular spectrum of the scattered light is given by [17]

$$I_{SC}(\theta,\phi) = \frac{k^4 V^2 |m-1|^2}{8\pi^2 s^2} I_o |R(\theta,\phi)|^2 \left(1+\cos^2\theta\right) \quad (11)$$

where V is volume of the particle, s is the distance from the scatter to the detector, $k = 2\pi n/\lambda$ and $R(\theta,\phi)$ is the form factor

$$R(\theta,\phi) = \frac{1}{V}\int B \exp\left(i2kb\sin\left(\frac{\theta}{2}\right)\right) db \quad (12)$$

which is an integration of slices perpendicular to the bisectrix, each slice having an area B and a thickness db. The form factor for a randomly oriented particle is obtained through integration over the solid angles that the orientation of the particle can have with the incident beam, the scattering direction (θ,ϕ) and hence the bisectrix are fixed. The expression for the averaged $\overline{R^2}$ is given by

$$\overline{R^2}(\theta,\phi) = \frac{1}{4\pi}\int R^2(\theta,\phi,\theta',\phi')\, d\cos\theta' d\varphi' \quad (13)$$

where (θ',ϕ') is the angle of the particle relative to the fixed bisectrix. The key consequence of (12) and (13) is that

$$\overline{R^2}(\theta,\phi) = \overline{R^2}\left(2k\sin\frac{\theta}{2}\right) \quad (14)$$

is only a function of $2k\sin(\theta/2)$ for any particle because a common set of all different orientations of the particle are averaged to form $\overline{R^2}$, independent of scattering direction (θ, ϕ). Note, this is valid for randomly oriented particles of any shape, but not valid when particles are not randomly oriented. The scattered light intensity under this condition is given by

$$I_{SC}(\theta) = \frac{k^4 V^2 |m-1|^2}{8\pi^2 s^2} I_o \overline{R}^2 \left(2k\sin\frac{\theta}{2}\right)\left(1+\cos^2\theta\right) \quad (15)$$

due to the randomly oriented particles.

For a collection of particles of "size" r and a particle size distribution (PSD) given by $N(r)$, the scattered light intensity is

$$I_{SC}(\theta) \propto k^4\left(1+\cos^2\theta\right)\int r^6 \overline{R^2}\left(2k\sin\frac{\theta}{2}\right) N(r) dr. \quad (16)$$

From this, the necessary conditions for the application of the R–G approximation are that: 1) scattering is dominated by single scattering and 2) the rescaled spectra from different angles and wave vectors agree with each other, i.e., the rescaled plots of $I_{\rm SC}(\theta)/(I_o k^4(1+\cos^2\theta))$ versus $k\sin(\theta/2)$ for the different scattering angles should align.

III. Specimens and Experimental Method

A. Specimens

Three species of bacteria, *Pseudomonas aeruginosa* (*Pa*), *Staphylococcus aureus* (*Sa*), and *Bacillus subtilis* (*Bs*), were chosen for their differences in size and shape. *Pa* are Gram-negative aerobic rod-shaped bacteria. *Pa* are commonly found in soil and water and can inhabit the surfaces of plants and

animals. It is an opportunistic pathogen which can infect almost any human tissue although it rarely infects healthy tissues. From fluorescence spectroscopy studies, *Pa* are known to have siderophores which absorb at 400 nm [20], [21] *Sa* are aerobic to facultatively anaerobic, spherical-shaped, Gram-positive bacteria. These bacteria can form conglomerates such as pairs, chains, or grape-like clusters. *Bs* are aerobic to facultatively anaerobic Gram-positive, rod-shaped bacteria and often grow in long chains. *Bs* are an endospore-forming type of bacteria which produce endospores when the ambient conditions are not suitable for growth or reproduction. Malachite green with safranin-counter staining was performed to verify that at the time of the measurements, the *Bs* samples were almost entirely vegetative cells with almost no endospores present.

The bacteria were grown at 37°C for 18 h on agar plates. After incubation and growth, the bacteria were harvested by adding 20 mL of sterile 0.45% saline solution directly onto the cultures and the bacterial colonies scraped into the solution under aseptic conditions avoiding disruption of the agar surface. The concentrated bacterial solutions were then diluted with sterile, 0.9% saline to the specific optical densities used in this study and transferred to 1×1 cm quartz cuvettes. Scattering and transmission measurements were performed at room temperature within 2–4 h of removing the specimens from the growth media. For each of the bacteria, the transmission and scattered light intensities were measured for a range of concentrations and optical densities were computed using a saline cuvette as a reference. Use of a saline cuvette reference corrected for reflections at the cuvette surfaces and scattering from the saline and cuvette. Specimens were diluted to concentrations which ranged from 1×10^7 to 5×10^8 microbes/mL. At the more dilute concentrations, most of the photons were either ballistic or underwent only single scattering.

1) Index of Refraction of Bacteria: The dielectric constant of bacterial cells is not well characterized. The index of refraction for the different components of mammalian cells has been measured and reported in the literature. [10] The data in [10] can be used to estimate the refractive index of the bacteria. Bacterial cells lack the higher index mitochondria and melanin of human cells and therefore the refractive index should be somewhat lower then for human cells. Using $n = 1.37$ for cytoplasm and $n = 1.39$ for nuclear material and assuming bacteria cells are approximately equal parts cytoplasm and nucleus, the index of refraction is estimated to be 1.38. By way of comparison, an index of 1.3886 was reported for marine bacteria. [22]

For bacteria in a saline solution, the relative index, $m = 1.38/1.33 = 1.038$ and the condition $|m-1| \ll 1$ is satisfied. For bacteria cells whose sizes are equal to, or a few times larger than the wavelengths of visible light, the condition $|m-1| \ll 1$ is still satisfied although $r > 1$ and the intermediate case is a valid approximation for calculating the scattering cross section.

2) Bacteria Size Distribution: The size distribution of the bacteria can be taken to be a Gamma function PSD with the form of [20], [23]

$$n(r) = \frac{r^{(1-3b)/b}}{(ab)^{1/b-2}\Gamma\left(\frac{1}{b}-2\right)} e^{-(r/ab)} \tag{17}$$

where a is the "effective" radius defined as the average of the radius weighted by the geometric cross section and given by

$$a = \frac{\int \pi r^3 n(r) dr}{\int \pi r^2 n(r) dr} \tag{18}$$

and b is the "effective" variance of the distribution, given by

$$b = \frac{\int (r-a)^2 \pi r^2 n(r) dr}{a^2 \int \pi r^2 n(r) dr}. \tag{19}$$

The mean radius $\langle r \rangle$ is

$$\langle r \rangle \equiv \frac{\int r n(r) dr}{\int n(r) dr} = a(1-2b) \tag{20}$$

and the maximum of the PSD is at $r_{\max} = a(1-3b)$.

3) Bacteria Concentration and Size by Electron Microscopy: In preparation for electron microscopy, the bacteria were first fixed which serves to stabilize the cells during the removal of water, then dehydrated using ethanol in a series of increasing concentrations, then mounted and sputter coated with a conducting high atomic number metal. The concentrations were estimated by uniformly distributing 50 μl volumes from two samples of each of the three bacteria on 25 mm diameter filters and using a scanning electron microscope to count the number of bacteria cells in randomly selected areas on the filters. Since the OD is linear in concentration, the concentrations of the remaining samples were calculated by comparing the OD at 0.5 μm for these samples with the OD of the samples subjected to microscopy. The calculated concentrations agreed closely with the relative concentrations determined by the (known) sample dilutions. Microscopic examination also provided an independent estimate of particle size and aspect ratio for the rod-shaped bacteria. Although the accuracy of this method for determining concentration was not expected to be high, the bacteria sizes calculated from transmission measurements were in very good agreement with microscopy.

The particle sizes observed under electron microscopy are: ~ 0.85 μm diameter for *Sa*; ~ 0.6 μm diameter and ~ 1.5 μm length for *Pa*; and ~ 1.0 μm diameter and ~ 3 μm length for *Bs*.

B. Experimental Apparatus

A schematic of the experimental setup for the transmission and scattering measurements is presented in Fig. 1. The light scattering and transmission measurements were performed in the visible region of the spectrum using a cw xenon lamp light source (Xenon Fiber Optic Light Source Model ILC201 from ILC Technology, Sunnyvale, CA) and a compact spectrometer/ charge-coupled device (CCD) detector combination (Ocean Optics Model PC 1000, Ocean Optics, Dunedin, FL). Illumination from the xenon lamp was coupled into a 500-μm diameter optical fiber and collimated upon exiting the fiber. The transmitted and scattered light was collected by a second 500-μm diameter quartz fiber positioned 4.0 cm from the entrance face of the cuvette. In order to prevent detector saturation, spectrally flat metallic filters were placed in the light path for reference intensity and transmission measurements. No filters were needed for the angular scattering measurements.

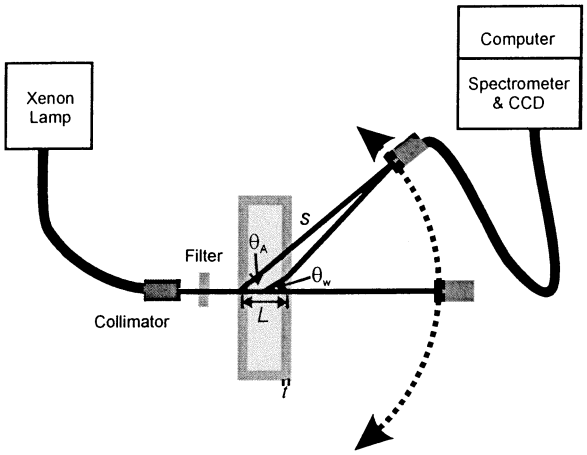

Fig. 1. Schematic of experimental apparatus for transmission and scattering measurements.

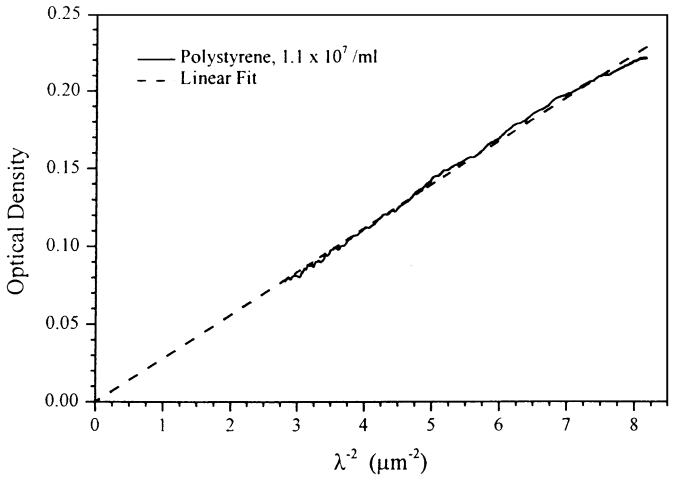

Fig. 2. Optical density of polystyrene 1.0 μm microspheres plotted as function of $1/\lambda^2$ and the corresponding linear fit.

The transmission of the metallic filters were independently measured with a Varian Cary 500 absorption instrument and, when appropriate, a filter correction was applied to the data. A 0.8-mm diameter aperture mounted in front of the collection fiber restricted the collection aperture angle to 1.35°. The spectral range of the transmission and scattering spectra were limited by the response of the spectrometer and CCD to 345–600 nm. The Ocean Optics spectrometer is mounted on a PCI expansion card installed in a personnel computer. The detector consists of a 1024 pixel linear array and 12-bit analog-to-digital converter. Data is transferred to the PC for storage and further processing. The integration time is programmable and multiple readouts of the CCD can be stored in memory and later summed to provide additional integration. Dark current is stored electronically and can be digitally subtracted from the data. In the data presented in this study, the PC 1000 was programmed to sum 600 frames, with a 10 ms readout time per frame, for a total integration time of 6 s per scan. For each measurement, 20 scans were acquired and averaged, for a total integration time of 120 s.

The collection fiber is mounted on a rotation stage which allows precise angular rotation of the collection fiber while maintaining a fixed distance to the entrance face of the sample cuvette. In this apparatus, the cuvette does not rotate with the detection fiber, but remains oriented normal to the incident light. The maximum measurable scattering angle is 48.7° (in water), limited by total internal reflection at the quartz/air interface. The minimum scattering angle is limited to 5° (in air) by the divergence of the illumination beam. At 5°, the intensity of the scattered light from the saline reference cuvette was less than 1% of the scattered light intensity from the weakest scattering bacteria specimen at this angle. Angular scattering spectra were collected in 2.5° steps between 5° and 20° (in air). In the geometry used in this apparatus (see Fig. 1), the relationship between the scattering angle in air and water is given by

$$\tan\theta_A = \frac{L}{2s}\tan\theta_w + \frac{t}{s}\tan\left[\arcsin\left(\frac{n_w}{n_g}\sin\theta_w\right)\right] + \left(\frac{s-L-2t}{s}\right)\tan\left[\arcsin\left(n_w\sin\theta_w\right)\right] \quad (21)$$

where s is the radius of the rotation stage (4.0 cm), θ_A is the angle of the stage, θ_w is the scattering angle in water, n_w and n_g are the indices of water and quartz, respectively, t is the thickness of the cuvette wall (1 mm), and L is the optical path length in the cuvette (10 mm).

IV. Validation With Polystyrene Microspheres

The system was tested by performing transmission and scattering measurements on 1.0 μm polystyrene latex microspheres (Sigma Aldrich). The microspheres (index of refraction = 1.59) were suspended in glycerin (index of refraction = 1.473) to satisfy the "soft" particle requirement of the IC (relative index = 1.08). Particle concentration was determined by a precise dilution of the known, initial concentration and was 1.1×10^7 particles/mL. The OD and the corresponding linear fit, of the polystyrene microspheres are plotted as function of $1/\lambda^2$ in Fig. 2 for λ in the range of 345 to 600 nm. As can be seen in Fig. 2, the OD is nearly linear in $1/\lambda^2$ and a linear least square fit with the intercept constraint to the origin gives a slope of 0.028 μm^2. From the known concentration (1.1×10^7/mL), path length (1 cm) and refractive index (1.59), the particle radius, calculated from (8), is 0.62 μm, in reasonable agreement with the 1-μm diameter specified by the manufacturer.

Angular scattering measurements were performed on the 1.0 μm polystyrene spheres. The seven detector angles in air, relative to the beam direction, varied from 5° to 20° in 2.5° steps (equivalent to scattering angles of 4.23°, 6.32°, 8.40°, 10.45°, 12.47°, 14.45°, and 16.39° in glycerin—see (21), with the substitution of the refractive index of glycerin for the refractive index of water). The most obvious features observed in the scattered intensity are due to the emission profile of the xenon lamp. A more hermeneutic view can be obtained by examining the scattered light intensities corrected for the lamp intensity, I_{sc}/I_o, which are plotted in Fig. 3. The most salient feature observed in the spectra plotted in Fig. 3 is a sharp increase in relative scattering intensity at wavelengths shorter than 430 nm.

The rescaled spectrum for the microspheres was calculated and is plotted in Fig. 4. A Gamma function PSD with an effec-

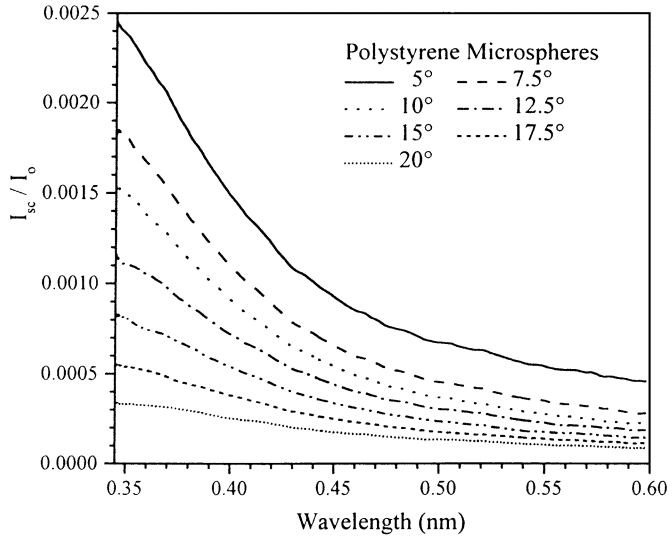

Fig. 3. Angular scattering intensity from the polystyrene microspheres at 4.23°, 6.32°, 8.40°, 10.45°, 12.47°, 14.45° and 16.39° (in glycerin). Intensity was normalized by the lamp intensity.

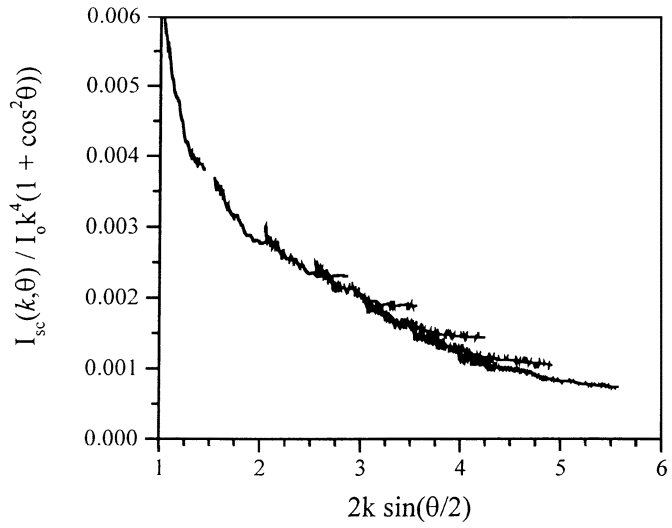

Fig. 4. Rescaled scattering intensity from polystyrene microspheres.

tive variance of 0.05 was assumed and the PSD was fitted with a least squares simplex algorithm using the scattering data between 480 and 600 nm. The calculated effective radius is 0.50 μm. Therefore, the mean radius is 0.45 μm and the maximum of the PSD is at 0.425 μm, in reasonable agreement with the manufacturer's specified 1.0-μm diameter. The PSD is plotted in Fig. 5. It is expected that for softer particles such as bacteria in water, the GRA of ADT and R–G theory for rescaled spectrum from multiple scattering angles should perform better.

V. Results

Transmission and scattering measurements were performed on five different concentrations of each of the three types of bacteria. The concentrations were chosen so that the two more dilute samples from each bacteria would exhibit primarily single scattering. This was experimentally verified.

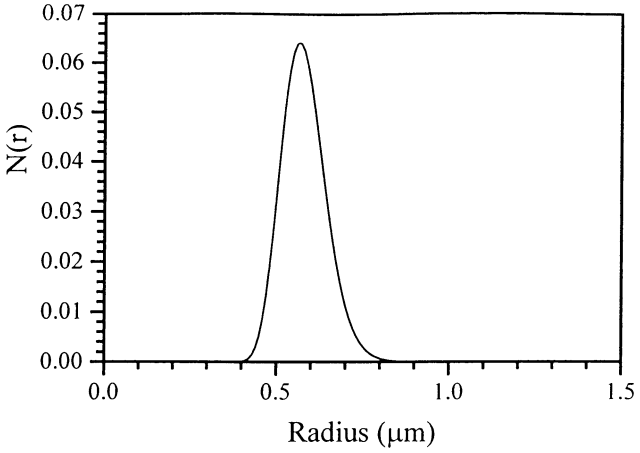

Fig. 5. PSD for polystyrene microspheres.

A. Transmission Measurements

Bacteria contain several native molecules that absorb in the blue and UV. These include flavins and nicotinamide adenine dinucleotide (NADH) in the blue and aromatic amino acids and nucleic acids in the UV. *Pa* also contains siderophores which fluoresces at 465 nm and have absorption bands at 400, 350, and 250 nm [21]. In the visible spectral region, absorption loses are considerably less than scattering loses. However, an absorption contribution was observed at shorter wavelengths, a region in which the OD was greater than that predicted by the IC.

It was also observed that in the experimental system used in this study, forward scattered light leakage became noticeable when the OD was greater than 1.8 for the smaller sized, *Pa* and *Sa* and 1.5 for the larger *Bs*. Forward scattered light leakage is scattered light collected by the finite acceptance angle of the detector and is in addition to the ballistic component.

From the transmission measurements, the IC was determined to be a valid approximation for the smaller sized *Pa* and *Sa*. For the larger sized *Bs* cells, the GRA can be used to fit the OD with a function quadratic in $1/\lambda^2$. The OD, plotted as function of $1/\lambda^2$ is shown in Fig. 6(a)–(c) for *Pa*, *Sa* and *Bs*, respectively. The corresponding linear fits for *Pa* and *Sa* and a quadratic fit for *Bs*, are also plotted in Fig. 6(a)–(c).

For all five concentrations of *Pa*, the OD is linear in $1/\lambda^2$ for the region between 550 and 600 nm, a region in which *Pa* does not absorb. A linear fit was performed on data in this range. Using the 0.4 aspect ratio (diameter/length) observed in microscopy the length and radius of the *Pa* was calculated from (9). All five concentrations gave nearly identical results of a 1.5 μm length and a 0.3 μm radius, in excellent agreement with the size observed under microscopy. Size results for the five *Pa* samples are summarized in Table II. The *Pa* absorption can be estimated from the difference between the measured OD and the IC approximation and can be observed in Fig. 6(a) at shorter wavelengths. The maximum absorption occurs below 400 nm and the absorption losses are less than 15% of the scattering losses.

Similarly for the *Sa*, the OD was linear in $1/\lambda^2$ for all five concentrations in the long wavelength region. Data in the range of 500 to 600 nm was used to generate the linear fit of the OD. All five concentrations of *Sa* give the same results for the radius, 0.43 μm, in good agreement with microscopy. The results for

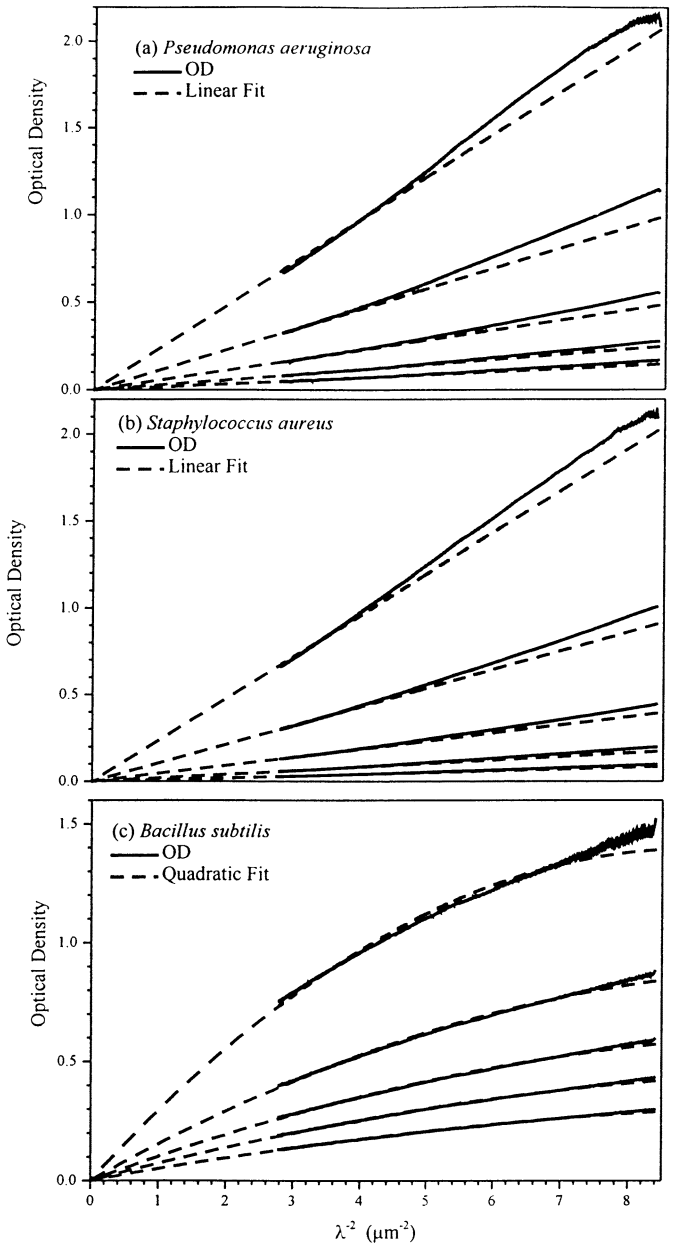

Fig. 6. Optical density of (a) *Pa*, (b) *Sa*, and (c) *Bs* plotted as function of $1/\lambda^2$ for five concentrations of each bacteria. A linear fit for the *Pa* and *Sa* and a quadratic fit for the *Bs* are shown.

TABLE II
PA SIZE CALCULATED FROM TRANSMISSION MEASUREMENTS

Concentration	Slope	Radius	Length
3.40×10^8 /ml	0.24602	0.30 μm	1.5 μm
1.65×10^8 /ml	0.11657	0.29 μm	1.5 μm
8.0×10^7 /ml	0.05725	0.30 μm	1.5 μm
4.1×10^7 /ml	0.02907	0.30 μm	1.5 μm
2.4×10^7 /ml	0.01723	0.30 μm	1.5 μm

the *Sa* samples are summarized in Table III. The presence of absorption can also be observed in *Sa* at shorter wavelengths

TABLE III
SA SIZE CALCULATED FROM TRANSMISSION MEASUREMENTS

Concentration	Slope	Radius
4.88×10^8 /ml	0.24032	0.43 μm
2.18×10^8 /ml	0.1078	0.43 μm
9.5×10^7 /ml	0.04661	0.43 μm
4.2×10^7 /ml	0.02054	0.43 μm
2.1×10^7 /ml	0.01013	0.43 μm

TABLE IV
BS SIZE CALCULATED FROM TRANSMISSION MEASUREMENTS

Concentration	A_0	A_1	Radius	Length
5.5×10^7 /ml	0.3113	-0.01737	0.49 μm	2.5 μm
3.0×10^7 /ml	0.16039	-0.00722	0.49 μm	2.4 μm
2.0×10^7 /ml	0.10604	-0.00452	0.49 μm	2.4 μm
1.46×10^7 /ml	0.07592	-0.00310	0.48 μm	2.4 μm
1.0×10^7 /ml	0.05222	-0.00212	0.49 μm	2.4 μm

but it is smaller than in the *Pa*. The maximum absorption loses are less than 10% of the scattering loses.

For the four more dilute concentrations of *Bs*, the form of the OD can be accurately described by (10) and the A_0/A_1 ratio is nearly equal for these four samples, varying from 24.6 for the most dilute to 22.2 for the second most concentrated. The highest concentration *Bs* sample could not be fitted by a quadratic in $1/\lambda^2$ as can be observed in Fig. 6(c). This may be due to the presence of a large amount of forward scattered light distorting the transmission measurements. From (1) and using an aspect ratio of 0.4, the average length of the *Bs* cells is 2.8 μm and the average radius is 0.56 μm, in agreement with the size observed under microscopy. Applying the IC and using A_0 for the slope of the OD, the *Bs* length and radius were calculated to be 2.4 μm and 0.49 μm, respectively. This value is slightly smaller than the value calculated from the GRA. The *Bs* size calculated from the GRA and the IC are presented in Table IV.

B. Angular Scattering Measurements

Scattering measurements were performed at seven detector angles which varied from 5° to 20° in 2.5° steps (equivalent to scattering angles in water of 4.63°, 6.93°, 9.21°, 11.46°, 13.69°, 15.88°, and 18.03°-see (21) and Fig. 1).

The ratio of scattered light intensity to incident intensity are plotted in Fig. 7(a)–(c) for the most dilute concentrations of *Pa*, *Sa*, and *Bs*, respectively at the seven angles. The salient features which can be observed in Fig. 7(a)–(c) are: 1) I_{sc}/I_o increases for shorter wavelengths—the increase is more rapid at smaller angles; 2) for the larger sized *Bs*, the decreases in intensity with angle is greater as compared to the smaller sized *Sa* and *Pa*; and 3) at the large angles, I_{sc}/I_o increases at shorter wavelengths for the *Sa* but not for the *Bs* or *Pa*.

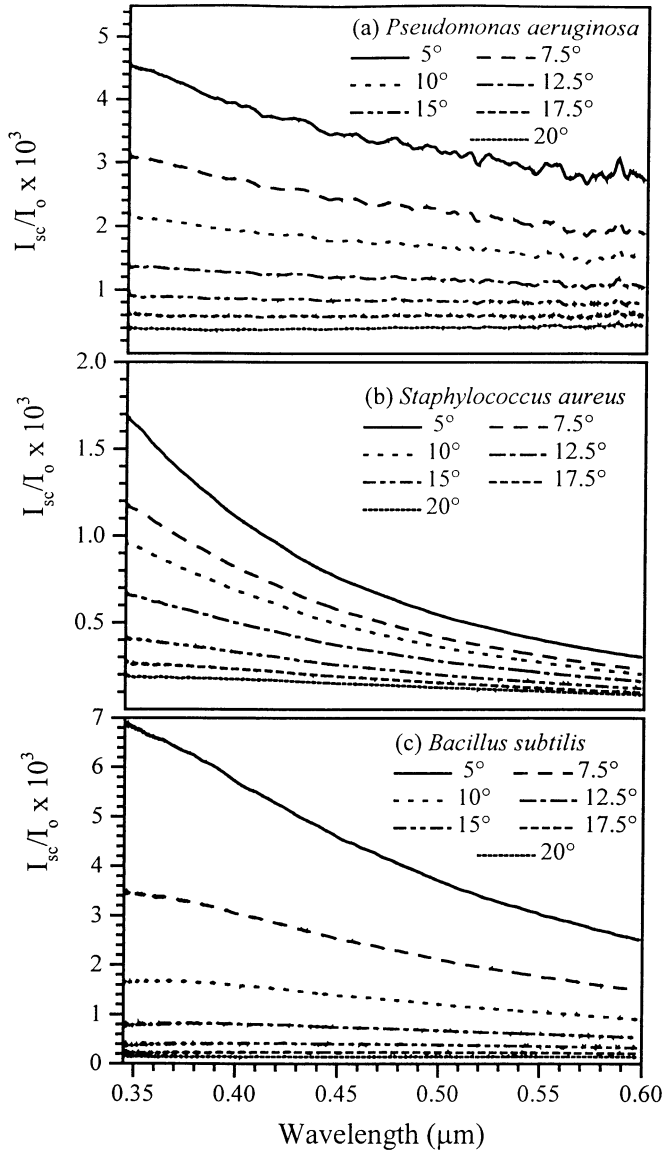

Fig. 7. Angular scattering intensity from most dilute concentrations of (a) *Pa*, (b) *Sa*, and (c) *Bs* corrected for lamp intensity at angles of 4.63°, 6.93°, 9.21°, 11.46°, 13.69°, 15.88°, and 18.03° (in water).

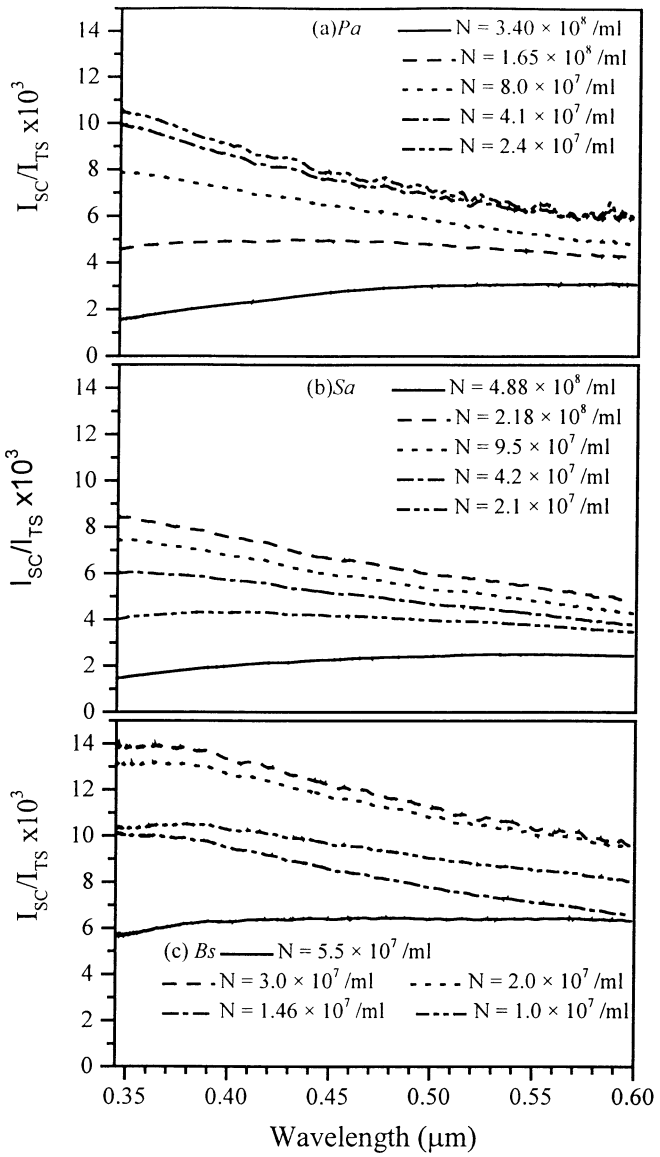

Fig. 8. Scattering intensity at 5° (in air) divided by total scatter light for (a) *Pa*, (b) *Sa*, and (c) *Bs* for five concentrations of each bacteria.

For single scattering, the form factor and, thus, the shape of the angular distribution of scattered light is independent of particle concentration. Therefore, at a given angle, the ratio, $I_{\rm SC}/I_{\rm TS}$, is independent of concentration. A comparison of $I_{\rm SC}/I_{\rm TS}$ for the different concentrations gives a measurement of the extent of multiple scattering and can be used to determine if single scattering dominates. Therefore, prior to analyzing the rescaled spectra, the angular scattering was examined to determine which specimen concentrations exhibited primarily single scattering. The $I_{\rm SC}/I_{\rm TS}$ ratio at 5° for the three different bacteria species are plotted in Fig. 8(a)–(c). Examination of Fig. 8(a) shows that the $I_{\rm SC}/I_{\rm TS}$ ratio for the two most dilute *Pa* concentrations are equal at longer wavelengths and nearly equal at shorter wavelengths, indicating that for these concentrations, mostly single scattering is occurring. $I_{\rm SC}/I_{\rm TS}$ for each of the three higher concentrations differ significantly from each other—an indication of multiple scattering. For the two most dilute *Sa* samples, plotted in Fig. 8(b), the $I_{\rm SC}/I_{\rm TS}$ ratios have the same shape, however, they differ by approximately 10%. The $I_{\rm SC}/I_{\rm TS}$ ratio for the two most dilute *Bs* concentrations are equal at longer wavelengths and close in value at shorter wavelengths [see Fig. 8(c)] indicating that, for these two samples, mostly single scattering is occurring. That the $I_{\rm SC}/I_{\rm TS}$ ratios are not exactly equal may be due to a small amount of double scattering. *Sa* and *Bs* are not uniformly distributed throughout the cuvette, but occur in clusters and chains, respectively, therefore, a photon which is scattered once is more likely to be scattered a second time and the number of double scatters may be higher then would be expected from a uniformly distributed bacteria population.

The rescaled spectra for the most dilute concentrations of *Pa*, *Sa*, and *Bs* are plotted in Fig. 9(a)–(c), respectively. The *Pa* spectra shows very good alignment at shorter wave vectors for all angles. At longer wave vectors, the alignment was not quite as good and the scattered intensity was slightly more at small

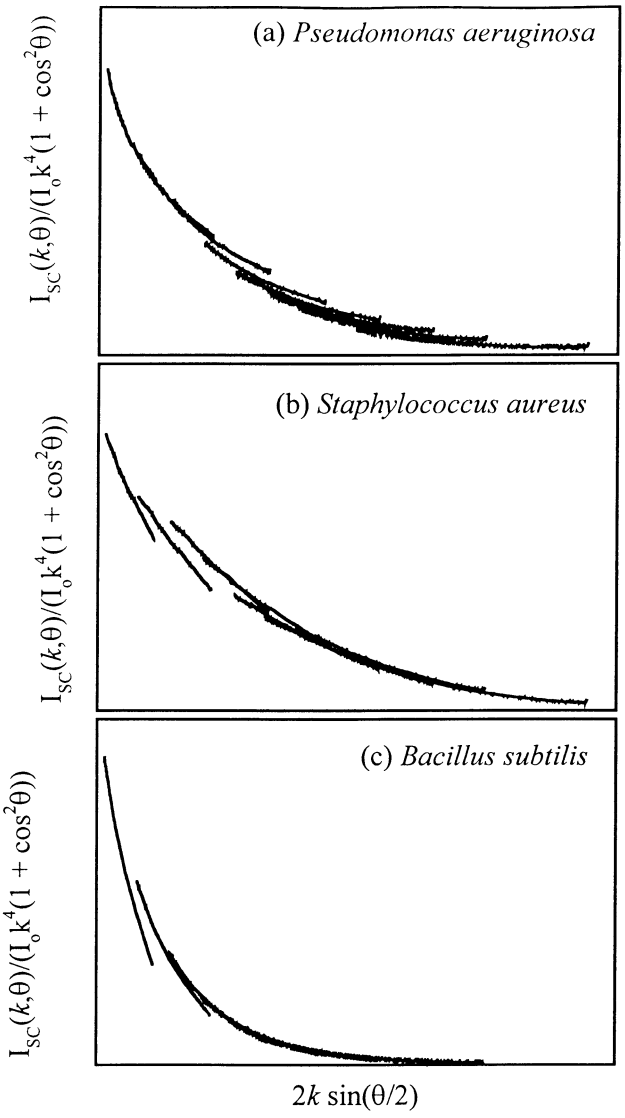

Fig. 9. Rescaled scattering intensity for the most dilute samples of (a) *Pa*, (b) *Sa*, and (c) *Bs*.

angles than at large angles for the same rescaled wave vector. This may be attributed to either the presence of weak absorption, or to a larger refractive index, at shorter wavelengths. Both the *Sa* and *Bs* spectra show very good alignment at larger angles [see Fig. 9(b) and (c)]. At smaller angles (5° and 7.5° for *Sa* and 5° for *Bs*) the spectra did not align nearly as well, with the scattered light intensity being weaker at small angles than expected from theory. This may be attributed to a small number of double scattering events which would increase the angular spread of the scattered light. Although the *Sa* had the lowest OD of the three bacteria and, therefore, was least likely to exhibit multiple scattering, the presence of clusters can increase the likelihood of double scattering as the distance between bacteria cells is reduced inside the cluster. The *Bs* which occur in long chains also exhibit weaker scattering at small angles than theory predicts. On the other hand, the *Pa*, which occur either singly, or in chains of no more than two or three bacteria cells, had excellent alignment at small angles.

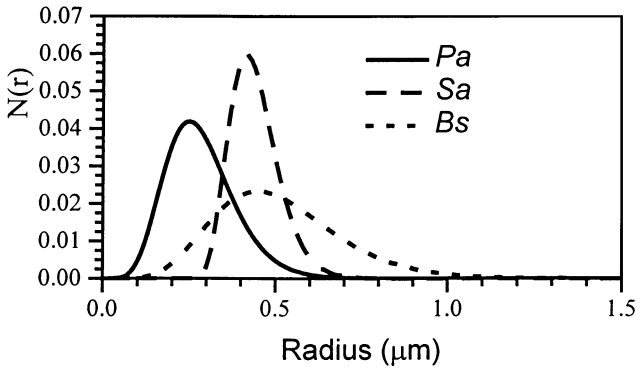

Fig. 10. PSD for radii of *Pa*, *Sa*, and *Bs*.

TABLE V
BACTERIA SIZE AS DETERMINED BY ANGULAR SCATTERING SPECTRA

	Concentration	Mean Radius	Mean Length
Pa	2.4×10^7 /ml	0.28 μm	1.4 μm
Sa	2.1×10^7 /ml	0.39 μm	---
Bs	1.0×10^7 /ml	0.51 μm	2.56 μm

A least square fitting using a simplex algorithm was also used to determine the particle radius and the aspect ratio for the rod-shaped bacteria. For the assumed Gamma function PSD, with an effective variance of 0.1, the results of the fitting algorithm give an aspect ratio (diameter/length) for the *Pa* of 0.4. The "effective" half length and offset are 0.89 μm and 10^{-5} μm, respectively. For an effective variance of 0.1, the mean length of the *Pa* is 1.4 μm and the mean radius is 0.28 μm. For the *Sa*, the fitting algorithm gives an "effective radius" of 0.25 μm and an offset of 0.24 μm for a mean radius of 0.39 μm. The fitting algorithm applied to the *Bs* gives an "effective length" of 3.2 μm and an aspect ratio of 0.4. Therefore, the mean length and radius of the *Bs* are 2.56 and 0.51 μm, respectively. The PSD for the radii of the three bacteria species are plotted in Fig. 10. The bacteria sizes as determined by angular scattering are summarized in Table V.

VI. CONCLUSION

This work has demonstrated the strength of light scattering determining size, shape and PSD of small particles. Our research has shown that light scattering can be an effective tool for measuring the size and shape of bacterial cells *in situ* and possibly provides a method to monitor the environment for microbial contamination. Excellent agreement is achieved between particle size retrieved from: the GRA applied to transmission measurements; PSD from the R–G approximation applied to the angular scattering spectra; and those from scanning electron microscopy. The bacteria sizes as measured by these three methods are summarized in Table VI. The transmission measurements from a range of concentrations can be used to measure the sizes of bacteria cells.

TABLE VI
SUMMARY OF MEAN SIZE OF BACTERIA FROM THE THREE TYPES OF MEASUREMENTS

	Electron Microscopy		Transmission Measurements		Angular Scattering	
	Radius (μm)	Length (μm)	Radius (μm)	Length (μm)	Radius (μm)	Length (μm)
Pa	0.3	1.5	0.30	1.5	0.28	1.4
Sa	0.425	-	0.43	-	0.39	-
Bs	0.5	3	0.49	2.4	0.51	2.56

ACKNOWLEDGMENT

The authors thank D. Breger and the Lamont–Doherty Earth Observatory for providing access to the electron microscope facilities.

REFERENCES

[1] P. J. Wyatt, "Differential light scattering: A Physical method for identifying living bacterial cells," *Appl. Opt.*, vol. 7, no. 10, pp. 1879–1896, 1968.
[2] A. L. Koch and E. Ehrenfeld, "The size and shape of bacteria by light scattering measurements," *Biochim. Biophys. Acta.*, vol. 165, no. 2, pp. 262–273, 1968.
[3] A. L. Koch, "Theory of the angular dependence of light scattered by bacteria and similar-sized biological objects," *J. Theor. Biol.*, vol. 18, no. 1, pp. 133–156, 1968.
[4] P. J. Wyatt, "Identification of bacteria by differential light scattering," *Nature*, vol. 221, no. 187, pp. 1257–1258, 1969.
[5] ——, "Cell wall thickness, size distribution, refractive index ratio and dry weight content of living bacteria (Staphylococcus aureus)," *Nature*, vol. 226, no. 242, pp. 277–279, 1970.
[6] P. J. Wyatt and D. T. Phillips, "Structure of single bacteria from light scattering," *J. Theor. Biol.*, vol. 37, no. 3, pp. 493–501, 1972.
[7] J. Murray, D. W. Hukins, and P. Evans, "Application of Mie theory and cubic splines to the representation of light scattering patterns from bacteria in the logarithmic growth phase," *Phys. Med. Biol.*, vol. 24, no. 2, pp. 408–415, 1979.
[8] B. V. Bronk, W. P. Van de Merwe, and M. Stanley, "In vivo measure of average bacterial cell size from a polarized light scattering function," *Cytometry*, vol. 13, no. 2, pp. 155–162, 1992.
[9] W. P. Van de Merwe, Z. Z. Li, B. V. Bronk, and J. Czege, "Polarized light scattering for rapid observation of bacterial size changes," *Biophys. J.*, vol. 73, no. 1, pp. 500–506, 1997.
[10] A. Brunsting and P. F. Mullaney, "Differential light scattering from spherical mammalian cells," *Biophys. J.*, vol. 14, no. 6, pp. 439–453, 1974.
[11] J. R. Mourant, M. Canpolat, C. Brocker, O. Esponda-Ramos, T. M. Johnson, A. Matanock, K. Stetter, and J. P. Freyer, "Light scattering from cells: The contribution of the nucleus and the effects of proliferative status," *J. Biomed. Opt.*, vol. 5, no. 2, pp. 131–137, 2000.
[12] L. T. Perelman, V. Backman, M. Wallace, G. Zonios, R. Manoharan, A. Nusrat, S. Shields, M. Seiler, C. Lima, T. Hamano, I. Itzkan, J. Van Dam, J. M. Crawford, and M. S. Feld, "Observation of periodic fine structure in reflectance from biological tissue: A new technique for measuring nuclear size distribution," *Phys. Rev. Lett.*, vol. 80, no. 3, pp. 627–630, 1998.
[13] V. Backman, M. B. Wallace, L. T. Perelman, J. T. Arendt, R. Gurjar, M. G. Muller, Q. Zhang, G. Zonios, E. Kline, J. A. McGilligan, S. Shapshay, T. Valdez, K. Badizadegan, J. M. Crawford, M. Fitzmaurice, S. Kabani, H. S. Levin, M. Seiler, R. R. Dasari, I. Itzkan, J. Van Dam, M. S. Feld, and T. McGillican, "Detection of preinvasive cancer cells," *Nature*, vol. 406, no. 6791, pp. 35–36, 2000.
[14] M. Frobisher, R. D. Hinsdill, K. T. Crabtree, and C. R. Goodheart, *Fundamentals of Microbiology*, 9th ed. Philadelphia, PA: W.B. Saunders Company, 1974.
[15] S. E. Harding, "Applications of light scattering in microbiology," *Biotechnol. Appl. Biochem*, vol. 8, no. 6, pp. 489–509, 1986.
[16] J. R. Mourant, J. P. Freyer, A. H. Hielscher, A. A. Eick, D. Shen, and T. M. Johnson, "Mechanisms of light scattering from biological cells relevant to noninvasive optical-tissue diagnostics," *Appl. Opt.*, vol. 37, no. 16, pp. 3586–3593, 1998.
[17] H. C. van de Hulst, *Light Scattering by Small Particles*. New York: Dover, 1981.
[18] P. Chylek and J. Li, "Light scattering by small particles in an intermediate region," *Opt. Commun.*, vol. 117, no. 5, pp. 389–394, 1995.
[19] M. Xu, M. Lax, and R. R. Alfano, "Anomalous diffraction of light with geometrical path statistics of rays and a Gaussian ray approximation," *Opt. Lett.*, vol. 28, no. 3, pp. 179–181, 2003.
[20] J. F. Hansen and L. D. Travis, "Light scattering in planetary atmospheres," *Space Sci. Rev.*, vol. 16, pp. 527–610, 1974.
[21] J. C. MacDonald and G. G. Bishop, "Spectral properties of a mixture of fluorescent pigments produced by Pseudomonas aeruginosa," *Biochim. Biophys. Acta.*, vol. 800, no. 1, pp. 11–20, 1984.
[22] M. Jonasz, G. Fournier, and D. Stramski, "Photometric immersion refractometry: A method for determining the refractive index of marine microbial particles from beam attenuation," *Appl. Opt.*, vol. 36, no. 18, pp. 4214–4225, 1997.
[23] J. E. Hansen and J. W. Hovenier, "Interpretation of the polarization of venus," *J. Atmospheric Sci.*, vol. 31, no. 4, pp. 1137–1160, 1974.

A. Katz received the Ph.D. degree in physics from The City University of New York, New York, NY, in 1989.

He is currently a Member of the research staff at the Institute for Ultrafast Lasers and Spectroscopy (IUSL) at The City College of New York.

Alexandra Alimova received the B.S./M.S. from Moscow Institute of Fine Chemical Technology, Moscow, Russia, in 1994.

She is currently a Research Associate at the IUSL.

Min Xu received the Ph.D. in physics from The City University of New York, in 2001.

He is currently a Research Associate at the IUSL. His main research interests include random processes and inverse problems such as particle sizing and photon migration turbid media.

Elizabeth Rudolph is currently pursuing the M.S. degree at the Department of Earth and Atmospheric Sciences, The City University of New York.

Mahendra K. Shah received the B.S. degree from the University of Bombay, Bombay, India, and the M.S. degree from Gujarat University, Ahmedbad, Gujarat, India.

He is currently the Supervisor of the Clinical Microbiology Laboratory at the New York Eye and Ear Infirmary (NYEEI), New York, NY, and an Assistant Professor at the New York Medical College, New York, NY.

Howard E. Savage received the B.S. and M.S. degrees from the University of Vermont, in 1964 and 1966, respectively, and the Ph.D. degree from Rutgers University, New Brunswick, NJ, in 1971.

He is an Assistant Professor at the New York Medical College, New York, and a Cell Biologist in the Department of Pathology at the NYEEI.

Richard B. Rosen received the B.A. from the University of Michigan, Ann Arbor, in 1975 and the M.D. from the University of Miami, Miami, FL, in 1985.

He currently holds appointments as an Assistant Professor of Ophthalmology at the New York Medical College and Director of Ophthalmology Resident Training at the NYEEI.

Steven A. McCormick received the B.S. degree from Duke University, Durham, NC, in 1980 and the M.D. degree from West Virginia University School of Medicine, Morgantown, 1984.

He is an Associate Professor of Pathology, Ophthalmology, and Otolaryngology/Head & Neck Surgery at New York Medical College and Director of Pathology and Laboratory Medicine at the NYEEI.

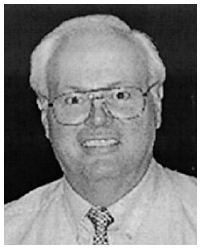

Robert R. Alfano (M'87–SM'89–F'01) received the B.S. and M.S. degrees in physics from Fairleigh Dickinson University, Teaneck, NJ, in 1963 and 1964, respectively, and the Ph.D. degree in physics from New York University, New York, in 1972.

He is a Distinguished Professor of Science and Engineering at the City College of the City University of New York, New York, and the Director of the Institute for Ultrafast Spectroscopy and Lasers, the NASA Center for Optical Sensing and Imaging, the DoD Nanophotonic Center, and the New York State Center for Advanced Technology in Ultrafast Photonics. Prior to joining the City College, he was a Research Physicist at General Telephone Research. He has published over 680 papers and holds 88 patents. His research during the past 35 years has been in the areas of ultrafast time-resolved spectroscopy, lasers, photonics, biomedical optics, condensed matter physics, and nonlinear optics. He has been one of the prime movers in optical biopsy and mammography. His group introduced fluorescence and Raman scattering to detect cancer and ballistic and snake photons for imaging in turbid media.

Prof. Alfano is a Fellow of the American Physical Society, the Optical Society of America, and the New York Academy of Sciences. He is a recipient of the Leonardo Da Vinci Award, the Lifetime Achievement Award in Biophotonics from Coherent, and was an Alfred P. Sloan Fellow.